Micromechanics simulations of fracture

van der Giessen, E.; Needleman, A.

Published in:
Annual Review of Materials Research

DOI:
10.1146/annurev.matsci.32.120301.102157

Annu. Rev. Mater. Res. 2002. 32:141–62
doi: 10.1146/annurev.matsci.32.120301.102157

MICROMECHANICS SIMULATIONS OF FRACTURE

E. Van der Giessen
Department of Applied Physics, University of Groningen, Nijenborgh 4, Groningen 9747, The Netherlands; e-mail: giessen@phys.rug.nl

A. Needleman
Division of Engineering, Brown University, Providence, Rhode Island 02912

Key Words dislocation plasticity, crack, fatigue, plastic zone

■ **Abstract** A fracture mechanics framework has been developed for predicting crack initiation and growth in full-scale components and structures from test specimen data. Much knowledge has also been gained about the mechanisms by which fracture occurs in a variety of materials. However, the development of quantitative connections between models of the physical processes of fracture and macroscale measures of fracture resistance is still at an early stage. A key difficulty is that fracture spans several length scales from the atomistic to the macroscopic scale. In this paper, some analyses are reviewed that use micromechanical modeling to predict fracture toughness from the physics of separation and plastic flow processes. Attention is confined to fracture by cleavage in metal crystals, under both monotonic and cyclic loading conditions. The role of models at the dislocation size scale in bridging the gap between atomistic and continuum descriptions is highlighted.

INTRODUCTION

Fracture is the process of separating a solid object into two or more pieces. Usually, but not always, this involves the nucleation and propagation of crack-like defects. Thus the key questions are, when will a crack nucleate and under what circumstances will the crack extend? As in most fields, growth is much better understood than nucleation, so that the focus in fracture studies has been on growth initiation and propagation of pre-existing cracks.

Fracture has been studied from two directions. In the engineering fracture mechanics community, where interest is in fracture-resistant design of structures and components, approaches have been developed that use experimentally measurable phenomenological parameters to characterize crack initiation and growth. In the materials science fracture mechanics community, where interest is in the development of fracture-resistant materials, the emphasis has been on the description of the physical processes of material separation. In the past two decades, much research has been focused on forging a link between these approaches in order to predict

fracture response from the physics of the processes involved. This effort constitutes the micromechanics of fracture, and numerical simulations play a key role.

The micromechanics of fracture is material dependent and, in general, involves a broad range of length and time scales. In this article, we review some recent work on modeling fracture in crystalline metals at room temperature, where dislocation glide is the dominant mechanism of plastic dissipation during crack growth. In these circumstances, there are two limiting behaviors. One is when few dislocations are generated and a cleavage crack propagates in a brittle manner. The other is when extensive dislocation activity precedes fracture, with the dislocations strongly relaxing the stresses near the crack tip, leading to continued blunting with cleavage fracture precluded. Although fracture ultimately does occur when the load increases, it then usually occurs by a mechanism involving the nucleation, growth, and coalescence of voids originating at second-phase particles or inclusions.

We focus here on an intermediate situation where cleavage fracture takes place in the presence of plastic flow. We first outline the various scales that are involved in the competition between crack growth by cleavage and plastic flow-induced crack blunting. For many of the length scales involved, continuum descriptions are appropriate, and we discuss descriptions of the state of stress and deformation near crack tips at decreasing length scales. This discussion points out that from the point of view of continuum mechanics, cleavage in the presence of plastic flow is somewhat paradoxical because continuum plasticity predicts stress levels at a blunted crack tip that are of the order of the flow strength—a stress level of the order of the theoretical strength, which is needed for cleavage, should not be attainable. The resolution of this paradox, we believe, lies in the dual role played by dislocations. On the one hand, dislocation motion shields the crack tip and increases the energy dissipation accompanying fracture. When averaging over many dislocations, this picture coincides with an appropriate continuum plasticity view. On the other hand, the local stress concentration associated with discrete dislocations in the vicinity of the crack tip can lead to stress levels of the magnitude of the cohesive strength, causing the crack to propagate. In conclusion, we discuss how the same duality can describe fatigue crack growth. We show that, without any additional modifications, models at this scale are able to predict fatigue thresholds as well as fatigue crack growth that is consistent with behavior commonly described by the Paris law (1).

GENERAL OVERVIEW OF FRACTURE MODELING

Scales in Fracture

The micromechanics of fracture attempts to link the macroscopic fracture resistance to the underlying physical mechanisms of irreversible deformation and material separation. In all cases, the actual separation process takes place by breaking atomic bonds.

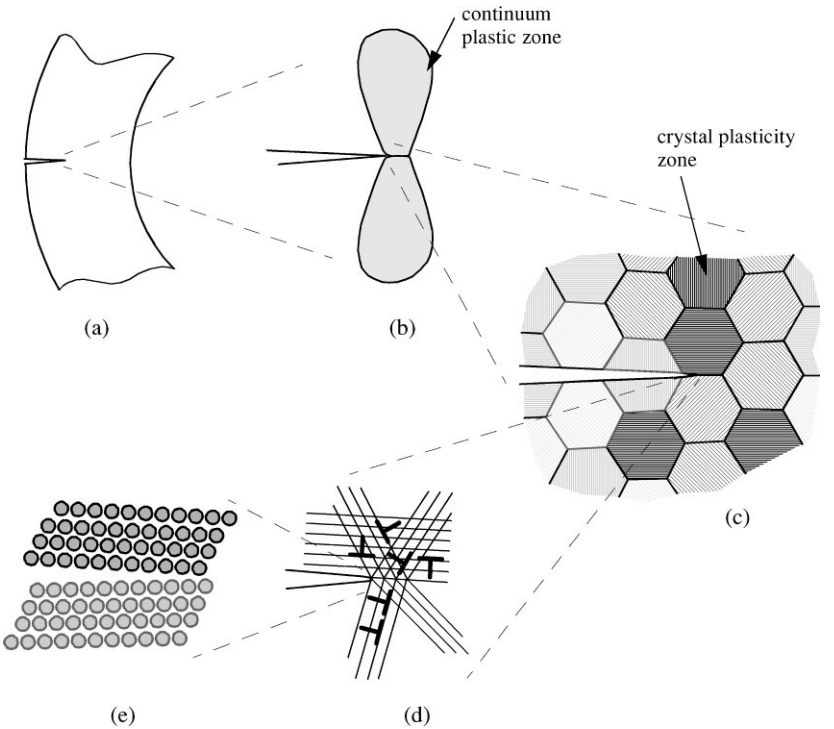

Figure 1 The various relevant scales that may determine the response of a crack in a macroscopic component. (*a*) The component scale; (*b*) the plastic zone governed by macroscopic continuum plastic flow; (*c*) the grain scale in a polycrystalline metal; (*d*) the scale of discrete slip planes and of individual dislocations; and (*e*) the atomic scale.

Figure 1 is an idealized illustration of the important length scales involved for cleavage crack growth in a relatively ductile polycrystalline metal. The relevant length scales range from that of the macroscale object to the atomic scale, including the various microstructural length scales in between that are associated with, for example, particles, grains, and defect structures.

The challenge lies in the fact that all scales are connected and all may contribute to the total fracture energy. It is worth noting that, although the atomistics of the separation of surfaces may contribute only a small fraction of the total energy release rate, it can still be controlling. This is because dissipative mechanisms can operate only if fracture is delayed sufficiently to allow them to come into play. Indeed, as pointed out by Rice & Wang (2), the surface energy can play a valve-like role. Surface energies are typically of the order of 1 J/m^2, whereas fracture energies for ductile crystalline metals can be on the order of 100 J/m^2 or greater.

The difference between the fracture energy and the surface energy is the plastic dissipation in the vicinity of the crack tip. The valve-like role of the surface energy emerges because relatively small increases in surface energy can delay fracture sufficiently to result in large increases in plastic dissipation.

At a sufficiently large scale, crack tip stress and deformation fields can be described in terms of a macroscopic, and often isotropic, continuum. Both elastic and (strain-hardening) plastic solids predict stress and strain fields at a tensile crack that share several key characteristics: (*a*) The stresses are singular (when the crack is modeled as being mathematically sharp), but the singularity depends on the strain-hardening characteristics of the material; (*b*) the stress distribution near the crack tip depends on the material properties but is independent of the loading conditions and the geometry; and (*c*) there is a single parameter characterizing the amplitude of the singularity that embodies the effects of geometry and loading.

At a smaller scale, the anisotropic nature of individual grains comes into play. This gives rise to stress and strain fluctuations with wavelengths equal to the grain size (Figure 1*c*). These fluctuations can be described using crystal plasticity models, which are conventional continuum constitutive relations but account for the discrete nature of the slip systems along which plastic flow occurs. As a consequence, the stress field near the crack tip is very different from the stress field for an isotropic solid.

Closer to the crack tip, the individual dislocations that mediate plastic flow come into play (Figure 1*d*). At this scale, energy dissipation is associated with the motion of large numbers of dislocations moving through the lattice. Each dislocation induces a localized stress concentration, which gives rise to large local stress fluctuations that vary as dislocations move and are generated from the crack tip itself or from nearby sources. In addition, dislocation structures can develop that have relatively long-range length stress fields, and these can increase the stress level in the vicinity of the crack tip.

The actual separation process takes place at the atomic scale (Figure 1*e*) in a region contained inside the dislocation plasticity zone. The stress field from the next higher-up scale induces local bonds between atoms to be stretched and broken when the stresses at this scale reach values on the order of the bond strength. This process may be assisted by other atoms that have diffused to the crack tip from the environment.

Many details are left out in the above discussion, but it emphasizes the fact that fracture, i.e., the creation of new surface, is highly localized at the atomic scale but is driven by the macroscopic applied load communicated to the atomic scale via stress fields on smaller and smaller length scales. It is the precise communication down these scales that determines whether crack growth occurs and how much energy is dissipated, see e.g., Hutchinson & Evans (3). The success of predictions of macroscopic fracture properties on the basis of atomic properties relies entirely on the accuracy with which the intermediate scales can be bridged. In transferring information between models at different size scales, there are subtle issues of

capturing the behavior at the smaller size scale in some appropriate average sense, particularly when defect structures are involved.

Continuum Modeling

All scales above the atomistic scale are analyzed within the framework of continuum mechanics. The way in which the continuum concept is used, however, differs from scale to scale. On the discrete dislocation scale, the continuum constitutive relation characterizes the elastic response of the material; plastic flow arises from the motion of discrete dislocations, modeled as continuum singular solutions to the field equations of linear elasticity. At the next higher scale, the discreteness of dislocations is ignored and plasticity is described by a continuum constitutive relation.

Because we only consider scales above the atomic scale, some of the basic concepts and equations used in the continuum modeling of fracture are briefly outlined. Attention is restricted to small strains and small rotations and to circumstances where material inertia plays a negligible role. Cartesian tensor notation is employed, with repeated lower case Latin subscripts implying a summation from 1 to 3. No summation is implied for Greek indices.

The position of a material point in the reference configuration, relative to a fixed Cartesian frame, is denoted by x_i. In the current configuration, at time t, this material point is at $\overline{x}_i$, so that the Cartesian components of the displacement field are $u_i(x_j, t) = \overline{x}_i(x_j, t) - x_i$. The displacements induce a strain tensor ϵ_{ij} according to

$$\epsilon_{ij} = \frac{1}{2}\left(\frac{\partial u_i}{\partial x_j} + \frac{\partial u_j}{\partial x_i}\right). \qquad 1.$$

The work associated with the motion of a material point is governed by the traction vector, the force per unit area, acting on a surface. If this surface normal is n_i, the traction vector is related to the stress state in the material by $T_i = \sigma_{ij}\, n_j$, where σ_{ij} are the components of the stress tensor. Equilibrium, or the balance of linear momentum, requires that

$$\frac{\partial \sigma_{ij}}{\partial x_j} = 0. \qquad 2.$$

The stress tensor is symmetric, $\sigma_{ij} = \sigma_{ji}$, as a consequence of the balance of angular momentum.

The above equations apply irrespective of what the continuum is supposed to represent. They need to be supplemented with constitutive equations that describe the material behavior. The simplest example is Hooke's law for elastic materials, where

$$\sigma_{ij} = L_{ijkl}\epsilon_{kl}, \qquad 3.$$

with L_{ijkl} the tensor of elastic moduli (e.g., C_{11}, C_{12}, C_{44} for a cubic material and E, ν for an isotropic material).

As is pointed out below, the discrete dislocation framework is based on an elastic continuum, for which the above equations form the set of governing equations. Plastic deformation then is the consequence of the motion of dislocations, and the path dependence of plastic flow emerges as a consequence of irreversibility in the evolution of the dislocation structure. In a conventional continuum description of plastic flow, the path dependence is directly incorporated into the stress-strain relation. Hence, the stress cannot be written as a direct function of strain. Instead, the plastic constitutive relation relates the stress rate to the strain rate, given the current state of the material. For the formulation of such a constitutive law, the strain rate is written, at each instant of time, as the sum of an elastic part and a plastic part,

$$\dot{\epsilon}_{ij} = \dot{\epsilon}^e_{ij} + \dot{\epsilon}^p_{ij} \qquad 4.$$

(here, and subsequently, a superposed dot denotes differentiation with respect to time). The elastic and plastic parts of the strain rate represent different mechanisms of deformation. Elastic deformation results from distortion of the crystal lattice, whereas plastic deformation by crystallographic slip, to a first approximation, leaves the lattice undisturbed. The elastic part of the strain rate is given by the time derivative of (3).

For application at the macroscopic scale (see, e.g., Figure 1*b*), where plastic flow is averaged over many grains, a widely used model is that of isotropic plasticity. The constitutive relation for the plastic part of the strain rate is

$$\dot{\epsilon}^p_{ij} = \frac{3}{2}\frac{\dot{\epsilon}_p}{\bar{\sigma}}\left[\sigma_{ij} - \frac{1}{3}\sigma_{kk}\delta_{ij}\right], \qquad 5.$$

where $\dot{\epsilon}_p$ is the Mises effective plastic strain rate, $\bar{\sigma}$ is the Mises effective stress, and the term in brackets defines the stress deviator.

At the smaller scale of individual grains (see, e.g., Figure 1*c*), plastic flow is anisotropic and takes place by simple shear on a specified set of slip planes. For single-crystal plasticity, the plastic strain rate is written as [see Asaro (4), Cuitiño & Ortiz (5), Bassani (6)]

$$\dot{\epsilon}^p_{ij} = \sum_\alpha \dot{\gamma}^{(\alpha)} \frac{1}{2}\left(s^{(\alpha)}_i m^{(\alpha)}_j + s^{(\alpha)}_j m^{(\alpha)}_i\right), \qquad 6.$$

where $s^{(\alpha)}_i$ specifies the slip direction for slip system α, and $m^{(\alpha)}_i$ the slip plane normal. A constitutive assumption that is often a reasonable approximation at ordinary temperatures, strain rates, and pressures is that the shear rate $\dot{\gamma}^{(\alpha)}$ depends on the stress only through the Schmidt resolved shear stress $\tau^{(\alpha)} = s^{(\alpha)}_i \sigma_{ij} m^{(\alpha)}_j$. For a rate-independent response, plastic flow occurs when $\tau^{(\alpha)} = g^{(\alpha)}$, where $g^{(\alpha)}$ is the current slip system hardness, which leads to a stress rate–strain rate relation of the form

$$\dot{\sigma}_{ij} = C_{ijkl}\dot{\epsilon}_{kl}, \qquad 7.$$

where the tensor of moduli C_{ijkl} depends on which slip systems are active, i.e., those for which $\dot{\gamma}^{(\alpha)}$ is non-zero. If none of them is active, C_{ijkl} reduces to the L_{ijkl} in (1). An isotropic plastic solid also has a stress rate–strain rate relation of the form (7) but with only two branches, one corresponding to plastic loading and the other to elastic unloading.

With constitutive equations as discussed above, boundary value problems can be solved. An important issue concerns the circumstances under which the solution is unique. For a strain-hardening Mises solid, the crack tip stress and strain fields are unique. On the other hand, as is discussed subsequently, the solutions for crack tip fields are not unique for nonhardening single crystals.

To model crack growth, we make use of cohesive surface theory [Needleman (7, 8)]. In a cohesive surface formulation, two constitutive relations are employed; one is a volumetric constitutive law that relates stress and strain, as discussed above, whereas the other is a traction versus displacement-jump relation across a specified set of surfaces. The cohesive surface constitutive relation embodies separation and deformation processes that occur on a size scale smaller than modeled by the volumetric constitutive relation.

CRACKS AND CONTINUUM PLASTICITY

Even though the focus here is on the role of plasticity near a crack tip, it is useful to recall the solution of the equations of linear elasticity in the vicinity of the tip of a stationary crack subject to tensile loading [see, e.g., Suresh (9) for a concise summary of continuum crack mechanics]. Sufficiently close to the crack tip

$$\sigma_{ij} = \frac{K_I}{\sqrt{2\pi r}} \Sigma_{ij}(\theta), \qquad 8.$$

where K_I is the tensile (mode I) stress intensity factor. Similar expressions are obtained for the stresses when the crack is subject to in-plane (mode II) or out-of-plane (mode III) shear loading. At the edge of an arbitrarily shaped crack in a three-dimensional solid, the stress state at each point is given by a superposition of the mode I, mode II, and mode III singular fields. However, we confine attention to planar cracks under mode I loading.

A key point is that the form of Equation 8 is independent of the remote loading. The effect of the remote loading and the geometry of the solid only enters through the amplitude K_I. The presumption underlying linear elastic fracture mechanics is that Equation 8 describes the stress and deformation field over a region that is larger than the region over which plastic flow and the physical processes of separation affect the stress state. When all nonlinear effects are confined to a region within which the stress state is described by Equation 8, small-scale yielding is said to occur. Under small-scale yielding conditions, the amplitude of the stress intensity factor K_I describes the loading conditions imposed on the region where plastic flow and separation are occurring. Hence, K_I serves as a characterizing parameter.

The applicability of K_I as a characterizing parameter in no way requires Equation 8 to describe the stress state near the crack tip where separation is taking place.

The elastic energy released per unit crack advance, $\mathcal{G}$, is proportional to K_I^2, so that the characterizing parameter can be taken as either K_I or $\mathcal{G}$. There are several advantages to using $\mathcal{G}$ rather than K_I as the characterizing parameter. As is discussed below, $\mathcal{G}$ also serves, in certain circumstances, as a characterizing parameter for plastic crack tip fields. In addition, $\mathcal{G}$ can be used as a characterizing parameter under mixed-mode conditions. For example, for interface cracks, the mismatch in elastic properties leads to mixed mode I–mode II loading conditions at the crack tip even if the remote loading is tensile.

When $\mathcal{G}$ serves as a characterizing parameter in the presence of plasticity, crack growth can be characterized in terms of a Griffith-Irwin type relation:

$$\mathcal{G} = \Gamma(\Delta a), \qquad 9.$$

where Δa is the increase in crack length. Because, for metals, the value of Γ is typically one to two orders of magnitude higher than the actual surface energy owing to plastic dissipation, there is a fundamental relation between a material's plastic properties and its crack growth resistance $\Gamma(\Delta a)$.

If plastic flow occurs over many grains in a polycrystal so that isotropic plasticity is a reasonable approximation [i.e., the near crack tip stresses are given by the HRR field, Hutchinson (10), Rice & Rosengren (11)],

$$\sigma_{ij} = \left(\frac{J}{cr}\right)^{1/(n+1)} \Sigma_{ij}(\theta; n). \qquad 10.$$

Here, it is assumed that the uniaxial stress-strain relation has the power law form $\epsilon \propto \sigma^n$; J is the value of Rice's (12) J-integral, which is equal to the energy release rate $\mathcal{G}$; and c is composed of a combination of numerical and material parameters. As for the elastic crack tip field (8), the function $\Sigma_{ij}(\theta; n)$ is independent of the remote loading conditions, provided the material exhibits strain hardening, i.e., $n < \infty$. In the absence of strain hardening, the near crack tip fields do not possess this autonomous character.

The characterization of crack tip fields by the HRR field, with $J = \mathcal{G}$ as the characterizing parameter, enables the determination of the function Γ from small fracture specimens where plastic flow is not confined to the crack tip region. In small-scale yielding, $J \propto K_I^2$, relating the amplitudes of the outer elastic and inner plastic stress fields. The use of J as characterizing parameter is not generally valid for crack growth or under cyclic loading conditions.

For a single crystal or for a grain in a polycrystal, the assumption of isotropy on which Equation 10 is based no longer holds and the near crack tip stress state is greatly affected by the discreteness of slip systems. For a nonhardening crystal, Rice (13) showed that a solution for the crack tip fields in a nonhardening crystal consists of angular sectors with constant Cartesian stress components. These results were extended to account for hardening by Saeedvafa & Rice (14), which gives rise to much more complicated stress fields, but the sector structure

remains. Uniqueness is not guaranteed for nonhardening crystals, and Drugan (15) has shown that alternative solutions are possible. In fact, the discrete dislocation results discussed in the next section were instrumental in guiding these solutions. A noteworthy feature of the nonhardening solutions is that stresses remain bounded at the crack tip and are on the order of the yield strength, although strain rates are singular.

The classical continuum crack tip fields set conditions on the region where fracture processes are taking place. They also can provide the appropriate parameters to define a material's fracture resistance but cannot predict it. Aims of the micromechanics of fracture include (*a*) calculating the dependence of a material's fracture toughness, $\Gamma(\Delta a)$, on its microstructure; (*b*) ascertaining the limits of applicability of the various characterizing parameters; and (*c*) providing a means of assessing a material's resistance to crack initiation and growth when the classical fracture mechanics characterization does not hold. Here, we focus on circumstances where the separation mechanism is cleavage and the mechanism of plastic flow is dislocation glide. We presume that small-scale yielding conditions hold so that the fracture toughness is characterized by $\Gamma(\Delta a)$.

To calculate the crack growth resistance, we use cohesive surface theory [Needleman (7, 8)]. The cohesive constitutive relation is formulated to represent separation by cleavage, and it contains two key parameters. One is the specific energy for cleavage, which is only one, usually small, contribution to the crack growth resistance. The largest contribution to the material's fracture toughness is generally the energy dissipated in the plastic zone, as described by the volumetric constitutive relation. The second key parameter is the cohesive strength. For cleavage, atomistic analyses indicate that the opening stress at a crack tip needs to reach the theoretical strength, which is of the order of $1/10$ of an elastic modulus. When classical continuum plasticity (whether isotropic or single crystal) is used to characterize the material behavior, such stresses are unattainable. Indeed, maximum attainable stress levels are an order of magnitude or more smaller than this [see e.g., Tvergaard & Hutchinson (16)].

Characterization of plastic flow in terms of discrete dislocation dynamics reduces the gap (Figure 1*d*). In the following, the focus is on the near-tip stress and deformation fields predicted by discrete dislocation plasticity and their implications for fracture behavior under both monotonic and cyclic loading.

DISLOCATION PLASTICITY AND CRACKS

At the length scale illustrated in Figure 1*d*, where individual dislocations can be distinguished, stress fields based on conventional continuum constitutive relations do not describe conditions near the crack tip because the dislocations carry a wildly fluctuating stress field. The dislocation stress fields are singular at the dislocation core and decay with the reciprocal distance from it, see e.g., Hirth & Lothe (17). In this section, we explore the extent to which these fluctuating fields average out to the continuum plasticity stress fields discussed above and consider

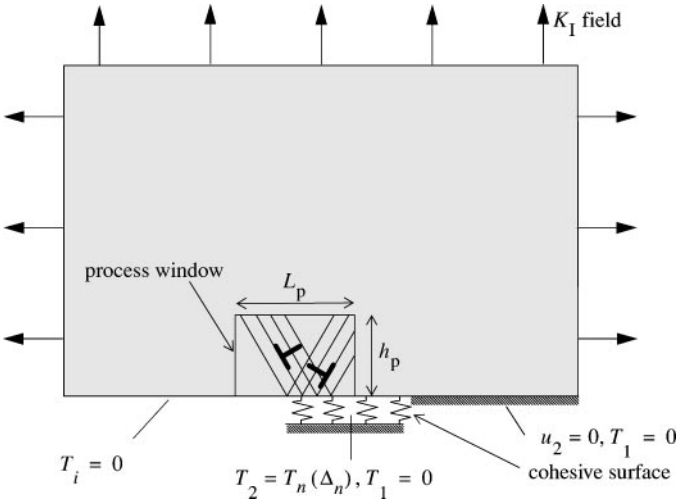

Figure 2 Small-scale yielding analysis under mode I conditions with discrete dislocations moving inside a process window. Because of symmetry, only half the problem needs to be analyzed. The cohesive surface ahead of the initial crack is used to describe crack growth.

the effect of the discrete dislocation–induced stress field fluctuations on the crack growth process. The discussion is based on the discrete dislocation analyses by Cleveringa et al. (18) and Van der Giessen et al. (19) for mode I loading conditions.

The calculations are carried out for small-scale yielding, and for computational reasons, plasticity is confined to a window around the initial crack tip. As illustrated in Figure 2, we define a set of two or three slip systems inside this window at an angle of $\phi^{(\alpha)}$ with respect to the crack plane. Two slip systems are necessary to allow for any mode of plastic deformation, while three slip systems mimic the excess of available slip systems in a real three-dimensional fcc crystal. Edge dislocations with Burgers vector $b^{(k)}$ ($k = 1, \ldots, N$) lie on these slip planes and can glide, be annihilated, be generated from Frank-Read sources, or be pinned at obstacles. All of these processes are governed by the Peach-Koehler force $f^{(k)}$ on the dislocation. In the analyses presented below, a linear drag relation is assumed for the glide velocity $v^{(k)}$ of the dislocation,

$$f^{(k)} = Bv^{(k)}, \qquad 11.$$

but more complicated relations are available and have been used in the literature (20). The sources in our two-dimensional analyses mimic Frank-Read sources and generate a dislocation dipole when the magnitude of the Peach-Koehler force exceeds a critical value of $b\tau_{\text{nuc}}$ during a period of time t_{nuc}. The obstacles, which could be small precipitates or forest dislocations, pin dislocations and release them once the Peach-Koehler force attains the obstacle strength $b\tau_{\text{obs}}$. Annihilation of

two dislocations with opposite Burgers vector occurs when they approach each other within a critical annihilation distance $L_e = 6b$.

The crack is initially sharp, and a cohesive surface is laid out in front of it. At the scale of interest here, the cohesive surface is taken to mimic atomic debonding. Therefore, the constitutive response of the cohesive surface is taken from the universal binding law, Rose et al. (21), and is specified by the following relation between the traction normal to the cohesive surface, T_n, and the separation Δ_n:

$$T_n(\Delta_n) = \sigma_{\max} \frac{\Delta_n}{\delta_n} \exp\left(1 - \frac{\Delta_n}{\delta_n}\right). \qquad 12.$$

As the cohesive surface separates, the magnitude of the traction increases, reaches a maximum, and then approaches zero to represent the formation of a traction-free crack. The strength $\sigma_{\max}$ and the corresponding separation δ_n characterize the fracture process and are taken to have values $\sigma_{\max} = 0.6$ GPa and $\delta_n = 4b$, giving a work of separation, $\phi_n = \exp(1)\, \sigma_{\max}\, \delta_n$ of 1.63 J/m^2. This value of the cohesive strength is about a factor of four smaller than the expected theoretical strength of aluminum and is used for numerical reasons because (*a*) the length scale over which large gradients occur is inversely proportional to the cohesive strength, so that a finer mesh is required for higher values of the cohesive strength; and (*b*) the number of dislocations increases with increasing cohesive strength, so that more dislocation interactions have to be computed and a larger process window is needed.

The boundary conditions for the problem sketched in Figure 2 are (*a*) the crack faces remain traction free, $T_I = 0$; (*b*) the displacements on the remote boundary are specified according to the well-known elastic singular field; and (*c*) for the symmetric mode I loading cases discussed here, Equation 12 is satisfied together with $T_t = 0$ on the crack plane ahead of the initial crack tip. The load level is thus characterized by the remote stress intensity factor K_I.

The analysis is carried out incrementally in time, with the loading prescribed to increase at a constant rate $\dot{K}_I$. With the dislocations treated as singularities in an elastic solid, the mathematical problem solved to determine the state of stress and deformation at each instant is nonlinear because of the cohesive surface and because of dislocation nucleation, annihilation, and interaction with obstacles. In addition, the highly fluctuating fields owing to the individual dislocations need to be resolved. The stress and deformation fields for individual edge dislocations in an infinite solid or in a half space are known analytically. The discrete dislocation stress and displacement fields, denoted by $\check{}$, are the superposition of the fields of the individual dislocations. The idea proposed by Van der Giessen & Needleman (22) is to make use of these solutions and to decompose the actual fields into a part $\check{}$ and a part $\hat{}$ that corrects for the actual boundary conditions. Details of the procedure for the incremental problem have been described by Cleveringa et al. (18) and are not repeated here. It is emphasized that the plastic flow characteristics near the crack tip, including the yield strength and hardening, and the crack growth behavior, including initiation and the growth rate, are outcomes of the analysis.

CRACKS AND DISLOCATIONS UNDER MONOTONIC LOADING

Fields Around Stationary Cracks

Stationary cracks are considered by Van der Giessen et al. (19) by using a very large value for the cohesive strength in Equation 12 so that T_n does not reach $\sigma_{\max}$. The computations are aimed at modeling metal single crystals with a high density of initial defects, which are modeled by a random distribution of point sources and obstacles in the process window. These represent Frank-Read segments and forest dislocations on slip planes with a normal out-of-the-plane of deformation. The two or three slip systems that are active in the analysis, however, are taken to be initially dislocation free. The calculations do not aim at modeling a specific material, but properties representative of aluminum are used. The elastic properties are taken to be isotropic, with Young's modulus $E = 70$ GPa and Poisson ratio $\nu = 0.33$. A representative value for the drag coefficient in Equation 11 is $B = 10^{-4}$ Pa s [Kubin et al. (23)], but measured values for nominally identical materials can differ by up to two orders of magnitude (24). The strength of the dislocation sources is randomly chosen from a Gaussian distribution with mean strength $\bar{\tau}_{\text{nuc}} = 50$ MPa and standard deviation $0.2\bar{\tau}_{\text{nuc}}$. The nucleation time for all sources is taken as $t_{\text{nuc}} = 10$ ns. All obstacles are taken to have the same strength $\tau_{\text{obs}} = 150$ MPa.

Figure 3 shows the stress distribution for a crystal in which there are three slip systems oriented at $\pm 60^\circ$ and 0° with respect to the crack plane. All three stress distributions exhibit large fluctuations, which are due to the singularities of the individual dislocations. In fact, the fluctuations shown are damped because of the way the contours are plotted on the finite element mesh that was used for the computation (80 by 80 elements in the process window).

It is remarkable, however, that three sectors appear around the crack tip in which the stresses, on average, look different from one another. This stress distribution is reminiscent of the analytical near-tip stress field obtained by Rice (13) on the basis of a continuum plasticity theory for nonhardening crystals. When his analysis for the true fcc crystal geometry is modified to account for the set of slip systems used by Van der Giessen et al. (19), four uniform stress sectors are obtained. The boundaries between these sectors are predicted to be 60°, 90°, and 120°, the first and last of which are consistent with the fields in Figure 3. Van der Giessen et al. (19) carried out a quantitative comparison by actually averaging the stresses inside the four mentioned sectors, and it was found that these average stresses agreed quite well with Rice's (13) continuum solution.

However, the discrete dislocation solution did not appear to agree with another element of Rice's (13) solution, namely that slip activity on the 0°-slip planes would concentrate in a kink band at 90°. The discrete dislocation results showed no evidence of this, as illustrated by the dislocation distribution shown in Figure 4. Subsequently, Drugan (15) carried out an analysis similar to Rice's (13), but without requiring a kink band. He found several solution families, including a family of

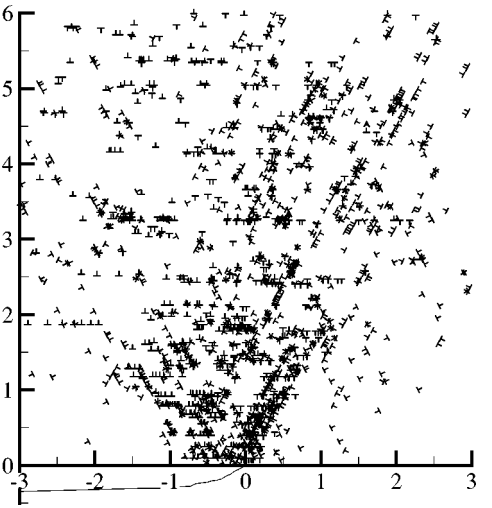

Figure 4 Dislocation distribution in the same crystal and at the same load level as in Figure 3. From Van der Giessen et al. (19).

solutions that involve only a slip band at $\theta = 60^\circ$, consistent with our discrete dislocation simulations. The solution that is closest to the discrete dislocation results is one where there are three sectors with boundaries at 60° and 105°. This solution is illustrated in Figure 5. Even though the 105° sector boundary is not obvious from Figure 3, averaging of the stress fields over these sectors showed very good agreement with this continuum prediction. Small differences in the exact average stress values are attributed to the fact that the continuum solution assumes no hardening, whereas some degree of hardening may occur in the discrete dislocation results. Even though real crystals will always show some degree of hardening, the

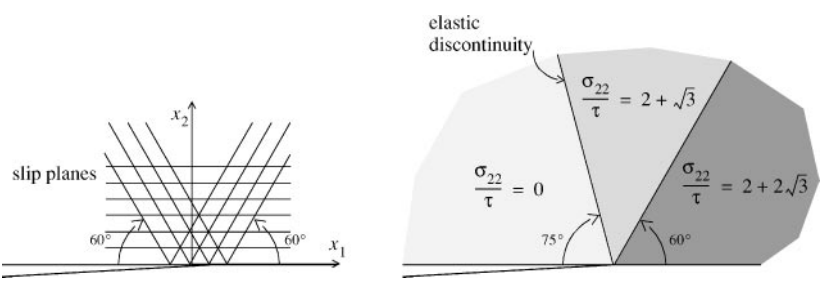

Figure 5 Opening stress states (σ_{22} normalized by the critical resolved shear stress τ) in the three sectors of Drugan's (15) solution.

main features of Drugan's (15) solutions have been seen in experiments by Crone & Shield (25).

Similar comparisons were carried out for another orientation of the crystal, Van der Giessen et al. (19), and for a crystal bonded to a rigid substrate, A. Nakatani, W. Drugan, A. Needleman & E. Van der Giessen (in preparation). In the cases analyzed, the continuum description allows for multiple solutions [Rice (13), Drugan (15)]. The discrete dislocation results help to identify one of the solutions. One possible explanation for the absence of kink bands in the discrete dislocation solutions of Van der Giessen et al. (19) is that lattice rotations are neglected; numerical continuum plasticity results by Cuitiño & Ortiz (5) suggest that this assumption may suppress the formation of kink bands. Another possibility is that kink bands would emerge for other discrete dislocation parameter ranges. Indeed, Kysar & Briant (27) used electron backscatter diffraction to observe rotation fields in pure aluminum crystals, and their observations are consistent with the kink band solution of Rice (13). They make the intriguing suggestion that kink band formation is associated with a very low density of obstacles, allowing dislocation glide over large distances.

Crack Growth

When averaging the discrete dislocation results over sectors to compare with the continuum plasticity predictions (19), the very near-tip region with a radius of 0.5 μm was excluded. The reason is that the stresses in this region are much higher than the sector averages (see Figure 3). In fact, the results of Cleveringa et al. (18) suggest that the stresses in this region can become high enough for crack advance by cleavage (although, for numerical reasons, the cohesive strengths in the calculations are smaller than representative of actual metal cohesive strengths). This is illustrated in Figure 6 for a case with two slip systems ($\pm 60^\circ$) and with a cohesive surface characterized by the values $\sigma_{\max} = 0.6$ GPa and $\delta_n = 4b$. For these parameter values, the stationary crack tip blunts because of dislocation activity (Figure 6*a*). The sector-average stresses at this instant are quite low, but the opening stress σ_{22} in a small region ahead of the crack reaches the cohesive strength. The crack then propagates until the crack tip arrives at a location where the near-tip opening stress is below the cohesive strength. Then, more dislocations are generated near the current tip, until the opening stress again reaches the strength (Figure 6*b*), and the crack jumps forward again. This process of blunting and crack jumping continues as the load increases, giving rise to a distinct *R*-curve behavior.

It is worth emphasizing that in the calculations by Cleveringa et al. (18) there is no emission of dislocations from the crack tip. This is in contrast to simulations, e.g., by Hirsch & Roberts (28) and by Nitzsche & Hsia (29), where it is assumed that dislocations can be emitted only by the crack tip. The same assumption has been made in the analyses of mode III cracks by Zacharopoulos et al. (30). This class of calculations aim at initially dislocation-free materials, such as silicon, where crack-tip emission is the key parameter in the transition from brittle fracture

(no dislocations) to ductile fracture accompanied by dislocation motion [see also Gumbsch et al. (20)]. However, the model considered here is intended to mimic a metal in which there is an initial distribution of dislocations that act as Frank-Read sources or as forest dislocation obstacles. The results shown in Figure 6 do depend sensitively on the initial density of sources and obstacles. If there are insufficient sources, the crack tip is not shielded and the crack advances in a brittle manner. In the absence of obstacles, on the other hand, the dislocations that are generated near the crack tip glide away from the tip, giving rise to continued crack tip blunting and no crack growth (18). It is because of the obstacles near the tip that dislocations cannot move far away from the crack tip. Some of these dislocations do not act to shield the crack, but rather aid in building up a high-stress region near the tip that drives the crack advance.

Not only do the results depend on the source and obstacle density, they also depend, in a restricted sense, on the source and obstacle distribution. It is evident that the precise stress distribution, as shown in Figure 6, depends on the positions of sources and obstacles. What is less evident, but was borne out by numerical simulations by Deshpande et al. (31), is that dislocation dynamics is chaotic. Perturbations in the source positions as small as $10^{-3}b$ give significant changes in the dislocation structure around the crack tip, and because the resulting stress state governs fracture, the fracture resistance can vary significantly.

A conclusion from the studies of Cleveringa et al. (18) is that dislocations play a dual role in fracture. On the one hand, dislocations are the vehicle for plastic deformation, and this reduces, on average, the stresses near the crack and provides a way to dissipate the energy flowing to the crack. On the other hand, dislocations can arrange themselves in structures, which lead to locally enhanced stress levels that can trigger crack growth. This stress enhancement is not modeled by conventional continuum plasticity. Which, if any, of the recently proposed nonlocal continuum crystal plasticity theories, e.g., by Shu & Fleck (32) or by Gurtin (33), provides an accurate description of the stress increase due to such dislocation structures remains to be determined.

FATIGUE CRACK GROWTH

The essence of fatigue crack growth, when the remote stress intensity cycles between $K_{\min}$ and $K_{\max}$, is that it occurs even when the driving force for crack growth is much smaller than what is needed for the same crack to grow under monotonic loading conditions. Typically, there is a threshold value of $\Delta K_{\mathrm{I}} = K_{\max} - K_{\min}$ below which cracks do not grow at a detectable rate. Above this threshold value, in the regime where the amount of crack growth per cycle, da/dN, is on the order of a few lattice spacings, there is a steep increase in da/dN with ΔK_{I}. For larger values of ΔK_{I}, the increase in da/dN becomes less steep and the Paris law regime (1) is entered where $da/dN \propto (\Delta K_{\mathrm{I}})^m$. Experimentally, the value of the Paris exponent m ranges widely; values of 2–4 are typically reported for ductile metals [e.g., Suresh (9), Ritchie et al. (34)], whereas values varying from 4.5 to as high as 40 have been

seen for intermetallics and nickel-based superalloy single crystals [Chan et al. (35), Mercer et al. (36)].

Fatigue requires irreversibility. Fatigue cannot occur in an elastic system because the state of the system then depends only on the current value of the loading parameter and not on its history. As a consequence, crack growth in an elastic system either occurs in the first cycle or does not occur at all. In addition, if the state of the system does not change during the unloading-reloading part of the cycle, fatigue crack growth is also precluded because the response then depends only on the peak value and not on how (or when) it is attained. Thus, the dissipation process during the unloading-reloading part of the cycle is key for fatigue.

The mechanism of fatigue crack growth in ductile solids is generally envisioned in terms of a deformation-driven blunting and sharpening mechanism proposed by Laird & Smith (37) and Neumann (38). For ductile metals, it involves nucleation of dislocations from the crack tip (or near the crack tip) leading to localized slip that is consistent with the typically observed fatigue striations, which are ripples seen on the fatigue fracture surface. Discrete dislocation models of fatigue crack growth have been developed, e.g., by Pippan and co-workers (39, 40) and by Wilkinson et al. (41), to represent this deformation-controlled fatigue crack growth mechanism. In these models, dislocations nucleate at or near the crack tip and then glide on specified slip planes. These models incorporate the crack growth mechanism as an ingredient of the model rather than have it emerge as a prediction of the analysis.

Continuum theories have tended to focus on the Paris law regime. Geometrical models presume that the crack growth rate is proportional to the cyclic crack opening displacement, which varies as $(\Delta K_{\mathrm{I}})^2$, giving a Paris exponent $m = 2$. Damage accumulation models, such as those of McClintock (42), Weertman (43), and Rice (44), give rise to a Paris exponent $m = 4$. Nguyen et al. (45) have carried out numerical calculations of fatigue crack growth in which the material was characterized by a conventional continuum plasticity model, and the fracture properties were embedded in a cohesive law that progressively softens and has loading-reloading hysteresis. They predicted Paris-like behavior with $m \approx 3$. These continuum models do not account for the wide range of Paris exponents observed experimentally. Furthermore, these models are restricted to the Paris law regime and do not predict the change in the dependence on ΔK_{I} that occurs near the fatigue threshold.

In the following, we discuss predictions for fatigue crack growth of Deshpande et al. (46, 47), which are based on the discrete dislocation formulation presented previously. The only difference in the fatigue calculations is that the remote stress intensity factor is taken to be a cyclic function of time. Crack growth along metal-ceramic interfaces was considered as well as in single crystals, but the discussion here focuses on the single-crystal results.

The calculations use both reversible and irreversible cohesive constitutive relations to account for cyclic loading in a vacuum and in an oxidizing environment, respectively. With a reversible cohesive constitutive relation, the only source of

irreversibility available to drive fatigue is that arising from dislocation motion. To model conditions as could occur in a perfect vacuum where there is no oxidation of the newly formed surface, the relation (12) is taken to be followed in a reversible manner. The other limiting case of complete oxidation of the newly formed surfaces, which is expected under normal atmospheric conditions, is modeled by linear unloading from and reloading to the monotonic cohesive law (12).

The Fatigue Threshold

Results from Deshpande et al. (46) are plotted in Figure 7*b* using the axes ΔK_{th} and K_{max}. The figure suggests that crack growth can occur under cyclic loading if and only if (*a*) the cyclic amplitude ΔK_I exceeds a critical value ΔK_{th}^* and (*b*) the maximum stress intensity K_{max} exceeds a critical value K_{max}^*.

The existence of these two parameters can be rationalized as follows:

1. For sufficiently low K_{max}, no dislocations are generated and the system is elastic. Therefore, for fatigue to occur with a reversible cohesive law, K_{max} must be at least large enough to nucleate dislocations in the surrounding field (this value depends on the source distribution). Effectively, there must be some minimum amount of plastic dissipation. Consequently, fatigue cannot occur below a minimum K_{max} denoted by K_{max}^*.
2. For $K_{\text{max}} \gg K_{\text{max}}^*$, interactions within the now dense dislocation structure act to retard dislocation motion. Accordingly, a minimum cyclic stress intensity factor range ΔK_I is needed to induce dislocation motion during unloading and reloading. Thus, in this regime, ΔK_I below a critical threshold value ΔK_{th}^* precludes crack growth.

Surface contact owing to the formation of oxide layers on the newly created surfaces strongly affects the behavior with the irreversible cohesive law in Figure 7. When the crack faces are in contact, the stresses in the vicinity of the crack tip are much reduced, inhibiting dislocation nucleation and glide as well as lessening the driving force for separation. As a consequence, crack propagation takes place only during the fraction of the fatigue loading cycle in which the crack faces at the tip are separated. The effective stress intensity range ΔK^{eff} responsible for crack growth is

$$\Delta K^{\text{eff}} = \begin{cases} K_{\text{max}} - K_{\text{op}} & \text{for } K_{\text{min}} < K_{\text{op}} \\ \Delta K_I & \text{for } K_{\text{min}} \geq K_{\text{op}}. \end{cases} \quad 13.$$

Curves of $\Delta K_{\text{th}}^{\text{eff}}$ are plotted in Figure 7*c* as a function of $R = K_{\text{min}}/K_{\text{max}}$. The absence of any load ratio effect for the irreversible cohesive law (compared with that seen in Figure 7*a*) suggests that the increase in ΔK_{th} with decreasing R is in fact a closure phenomenon; the fatigue threshold with the irreversible cohesive law is at a constant effective threshold stress intensity factor range ΔK_{th}^*. An approximate bilinear fit to the results of the computations is also shown in Figure 7. It should be emphasized that although $K_{\text{max}} \geq K_0$, which is a measure of the energy required to

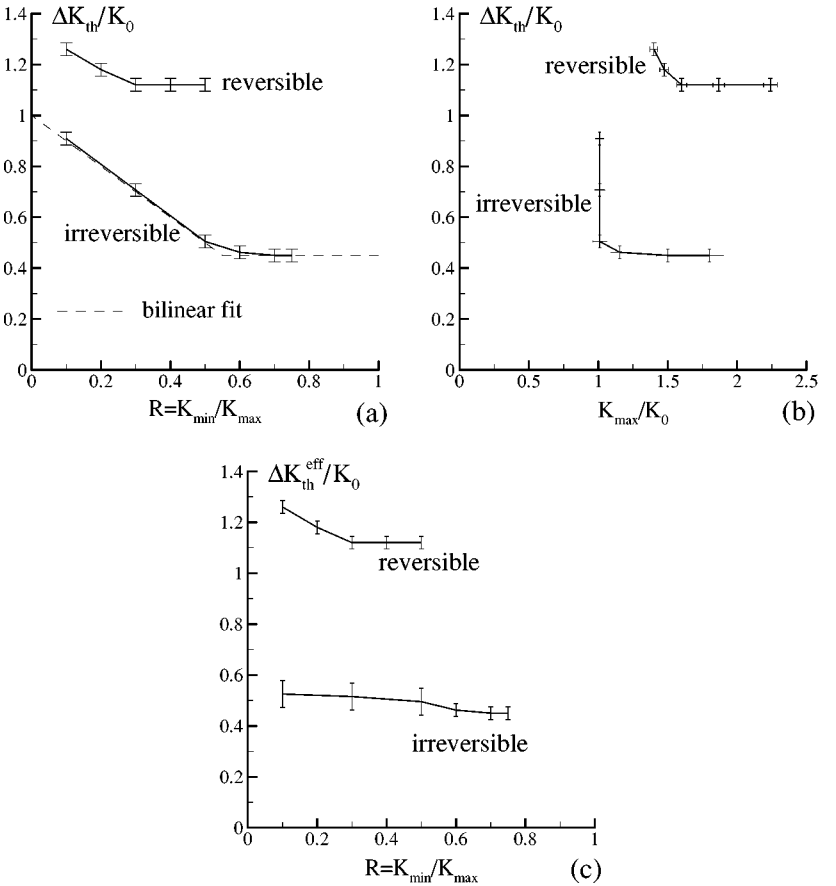

Figure 7 (*a*) Variation of ΔK_{th} with load ratio $R = K_{\min}/K_{\max}$. (*b*) ΔK_{th} as a function of the applied $K_{\max}$. (*c*) Load ratio dependence of the effective fatigue threshold $\Delta K_{\text{th}}^{\text{eff}}$, which is defined by Equation 13. The bars represent bounds on the appropriate quantities because ΔK_{th} was estimated by reducing the applied ΔK_I in discrete steps of $0.05K_0$. From Deshpande et al. (46).

create the new crack surface, crack growth occurs under cyclic loading with $K_{\max}$ much less than the K_I value needed for the same crack to grow under monotonic loading conditions.

The calculations modeling both perfect vacuum and oxidizing environmental conditions exhibit a dependence of the fatigue threshold on R. With a reversible cohesive law, this is an outcome of insufficient plasticity at low R values, whereas with an irreversible cohesive law, the R dependence is an outcome of crack closure at low values of R. For both cohesive laws, the fatigue threshold is insensitive to R for larger values of R.

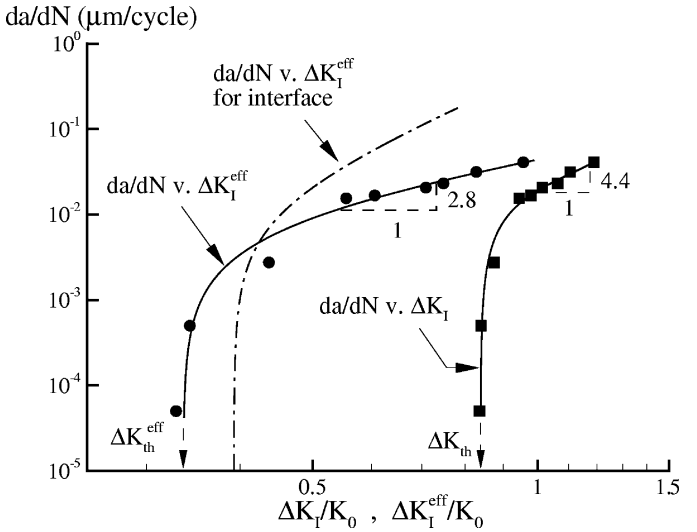

Figure 8 The cyclic crack growth rate da/dN versus $\Delta K_I/K_0$ and $\Delta K_I^{eff}/K_0$ for the mode I cyclic loading of a single crystal. For comparison purposes, a curve for an interface crack is also shown. The slopes of the curves marked correspond to the Paris law exponents for the curves fit through the numerical results. From Deshpande et al. (47).

The Approach to Paris Law Behavior

Curves of da/dN versus ΔK_I for a single crystal, taken from Deshpande et al. (47), are shown in Figure 8. The da/dN values plotted are averages over the number of cycles computed. This was generally 20 and 10 for low and high values of ΔK_I, respectively. There are two distinct regimes of behavior: a steeply rising $\log(da/dN)$ versus $\log(\Delta K_I/K_0)$ curve in the threshold regime followed by a more gradual slope in the Paris regime. The Paris exponent m in this case is $\approx$4.4. The cyclic crack growth rate da/dN is also plotted in Figure 8 as a function of ΔK_I^{eff}, with ΔK_I^{eff} calculated using Equation 13. The effect of crack closure is more pronounced at the lower values of ΔK_I so that ΔK_{th}^{eff} is much less than ΔK_{th}. Crack closure also results in an exponent $m \approx 2.8$ for the modified Paris relation

$$\frac{da}{dN} \propto \left(\Delta K_I^{eff}\right)^m . \qquad 14.$$

A fit da/dN versus $\Delta K_I^{eff}/K_0$ curve for an interface crack is also plotted in Figure 8. The interface calculations were performed for the configuration shown in Figure 2, modified by removing the symmetry and by replacing the cohesive relation (12) with one that allows for shear as well as normal decohesion. The effect of the mode mixity at the interface is to increase the fatigue threshold of the

interface crack but to reduce its resistance to cyclic crack growth at higher values of applied ΔK_I. This behavior is expected to be dependent on the degree of mode mixity and hence affected by the cohesive properties and the applied loading.

The form of the $\log(da/dN)$ versus $\log(\Delta K_I)$ curve seen experimentally, with a threshold and a Paris law regime, is captured in Figure 8. In the near-threshold regime, the $\log(da/dN)$ versus $\log(\Delta K_I)$ curve is steeply increasing as a significant proportion of the driving energy is going into the work of separation with only small amounts of plastic dissipation in the bulk material. With increasing ΔK_I, the plastic zone size increases, which results in increased plastic dissipation. This gives rise to the knee in the $\log(da/dN)$ versus $\log(\Delta K_I)$ curve, with the Paris law exponent m decreasing as the ratio of the plastic dissipation to the work of separation increases. This indicates a possible rationale for the high value of the Paris law exponent in intermetallics and superalloys and for the much lower value seen for ductile metals.

In the calculations of Deshpande et al. (47), rather uniformly spaced slip traces emerge in the wake of the propagating fatigue crack. Figure 9 shows contours of accumulated slip for a fatigue crack along a metal-ceramic interface. The deformation field is similar to that in the experiments of Laird & Smith (37) and Neumann (38) for cyclic crack growth in metals. In the calculations, as in the experiments, striations emerge as traces of concentrated slip on the newly created free metal

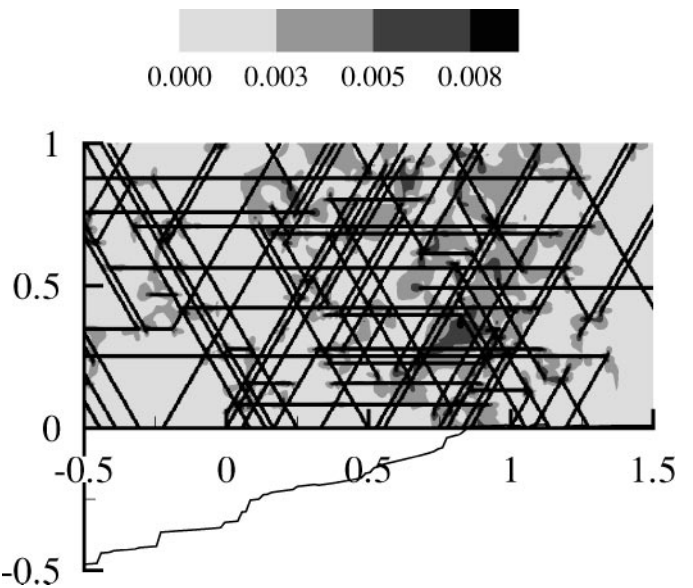

Figure 9 Contours of total slip showing the localized deformation pattern in the crack tip vicinity. All distances are in micrometers. The crack opening profile (displacements magnified by a factor of 20) is plotted below the x_1-axis. From Deshpande et al. (47).

surfaces. The striation spacing is of the order of the amount of crack growth per cycle in the Paris law regime and greater than the amount of crack growth per cycle in the near-threshold regime. The striations in Figure 9 most closely resemble type B striations according to the classification scheme of Forsyth (48).

Based on the experimental work of Laird & Smith (37) and Neumann (38), fatigue crack growth in ductile metals is often presumed to occur by an alternating slip mechanism, which is a deformation-controlled phenomenon that does not require high stresses. By contrast, in the framework of Deshpande et al. (46, 47), fracture is both a deformation and stress-governed phenomenon and takes place by a mechanism that is possible under both monotonic and cyclic-loading conditions. Furthermore, it is worth noting that striation formation is observed in fatigue crack growth at metal-ceramic interfaces (49), even though the kinematics of crack growth by an alternating slip mechanism is not clear for a crack growing along such an interface.

The calculations in Deshpande et al. (46, 47) give rise to crack growth under cyclic-loading conditions when the driving force is smaller than what is needed for the crack to grow under monotonic-loading conditions and hence exhibit fatigue. The origin of continued crack growth under cyclic loading lies in the irreversibility of dislocation motion. Under cyclic-loading conditions, as under monotonic-loading conditions, the locally high stress concentration ahead of the crack, mediated by the clustering of dislocations near the tip, plays a key role in the process of crack initiation and growth.

ACKNOWLEDGMENTS

A.N. is pleased to acknowledge support from the AFOSR MURI at Brown University on *Virtual Testing and Design of Materials: A Multiscale Approach* (AFOSR grant F49620-99-1-0272) and from the Materials Research Science and Engineering Center on *On Micro-and-Nano-Mechanics of Electronic and Structural Materials* at Brown University (NSF grant DMR-0079964).

The *Annual Review of Materials Research* is online at http://matsci.annualreviews.org

LITERATURE CITED

1. Paris PC, Gomez MP, Anderson WP. 1961. *Trend Eng.* 13:9–14
2. Rice JR, Wang J-S. 1989. *Mater. Sci. Eng.* A107:23–40
3. Hutchinson JW, Evans AE. 2000. *Acta Mater.* 48:125–35
4. Asaro RJ. 1983. *Adv. Appl. Mech.* 23:1–115
5. Cuitiño AM, Ortiz M. 1993. *Model. Simul. Mater. Sci. Eng.* 1:225–63
6. Bassani JL. 1994. *Adv. Appl. Mech.* 30: 191–258
7. Needleman A. 1987. *J. Appl. Mech.* 54: 525–31
8. Needleman A. 1990. *J. Mech. Phys. Solids* 38:289–324
9. Suresh S. 1998. *Fatigue of Materials*. Cambridge, UK: Cambridge Univ. Press
10. Hutchinson JW. 1968. *J. Mech. Phys. Solids* 16:13–31

11. Rice JR, Rosengren G. 1968. *J. Mech. Phys. Solids* 16:1–12
12. Rice JR. 1968. *J. Appl. Mech.* 35:379–86
13. Rice JR. 1987. *Mech. Mater.* 6:317–35
14. Saeedvafa M, Rice JR. 1989. *J. Mech. Phys. Solids* 37:673–91
15. Drugan W. 2001. *J. Mech. Phys. Solids* 49: 2155–76
16. Tvergaard V, Hutchinson JW. 1992. *J. Mech. Phys. Solids* 40:1377–97
17. Hirth JP, Lothe J. 1982. *Theory of Dislocations*. New York: Wiley. 2nd ed.
18. Cleveringa HHM, Van der Giessen E, Needleman A. 2000. *J. Mech. Phys. Solids* 48:1133–57
19. Van der Giessen E, Deshpande VS, Cleveringa HHM, Needleman A. 2001. *J. Mech. Phys. Solids.* 49:2133–53
20. Gumbsch P, Riedle J, Hartmaier A, Fischmeister HF. 1998. *Science* 282:1293–95
21. Rose JH, Ferrante J, Smith JR. 1981. *Phys. Rev. Lett.* 47:675–78
22. Van der Giessen E, Needleman A. 1995. *Model. Simul. Mater. Sci. Eng.* 3:689–735
23. Kubin LP, Canova G, Condat M, Devincre B, Pontikis V, Bréchet Y. 1992. *Solid State Phenomena* 23–24:455–72
24. Alshits VI, Indenbom VL. 1986. In *Dislocations in Solids*, ed. FRN Nabarro, 7:43–111.
25. Crone WC, Shield TW. 2001. *J. Mech. Phys. Solids* 49:2819–38
26. Deleted in proof
27. Kysar JW, Briant CL. 2002. *Acta Mater.* In press
28. Hirsch PB, Roberts SG. 1989. *Scripta Metall.* 23:925–30
29. Nitzsche VR, Hsia KJ. 1994. *Mater. Sci. Eng.* A176:155–64
30. Zacharopoulos N, Srolovitz DJ, LeSar R. 1997. *Acta Mater.* 45:3745–63
31. Deshpande VS, Needleman A, Van der Giessen E. 2001. *Scripta Mater.* 4:1047–53
32. Shu JY, Fleck NA. 1999. *J. Mech. Phys. Solids* 47:297–324
33. Gurtin ME. 2000. *J. Mech. Phys. Solids* 48: 989–1036
34. Ritchie RO, Yu W, Blom AF, Holm DK. 1987. *Fatigue Fract. Eng. Mater. Struct.* 10:343–62
35. Chan KS, Hack JE, Leverant GR. 1987. *Metall. Trans.* 18A:581–91
36. Mercer C, Soboyejo ABO, Soboyejo WO. 1999. *Acta Mater.* 47:2727–40
37. Laird C, Smith GC. 1962. *Philos. Mag.* 7:847–57
38. Neumann P. 1969. *Acta Metall.* 17:1219–25
39. Pippan R. 1991. *Acta Metall. Mater.* 39: 255–62
40. Riemelmoser FO, Gumbsch P, Pippan R. 2001. *Mater. Trans. JIM* 42:2–13
41. Wilkinson AJ, Roberts SG, Hirsch PB. 1998. *Acta Mater.* 46:379–90
42. McClintock FA. 1963. In *Fracture of Solids*, ed. DC Drucker, JJ Gilman, pp. 65–102.
43. Weertman J. 1966. *Int. J. Fract.* 2:460–67
44. Rice JR. 1967. Fatigue crack propagation, *ASTM STP* 415:247–309
45. Nguyen O, Repetto A, Ortiz M, Radovitzky RA. 2001. *Int. J. Fract.* 110:351–69
46. Deshpande VS, Needleman A, Van der Giessen E. 2001. *Acta Mater.* 49:3189–203
47. Deshpande VS, Needleman A, Van der Giessen E. 2002. *Acta Mater.* 50:831–46
48. Forsyth PJE. 1963. *Acta Metall.* 11:703–15
49. McNaney JM, Cannon RM, Ritchie RO. 1996. *Acta Mater.* 44:4713–28

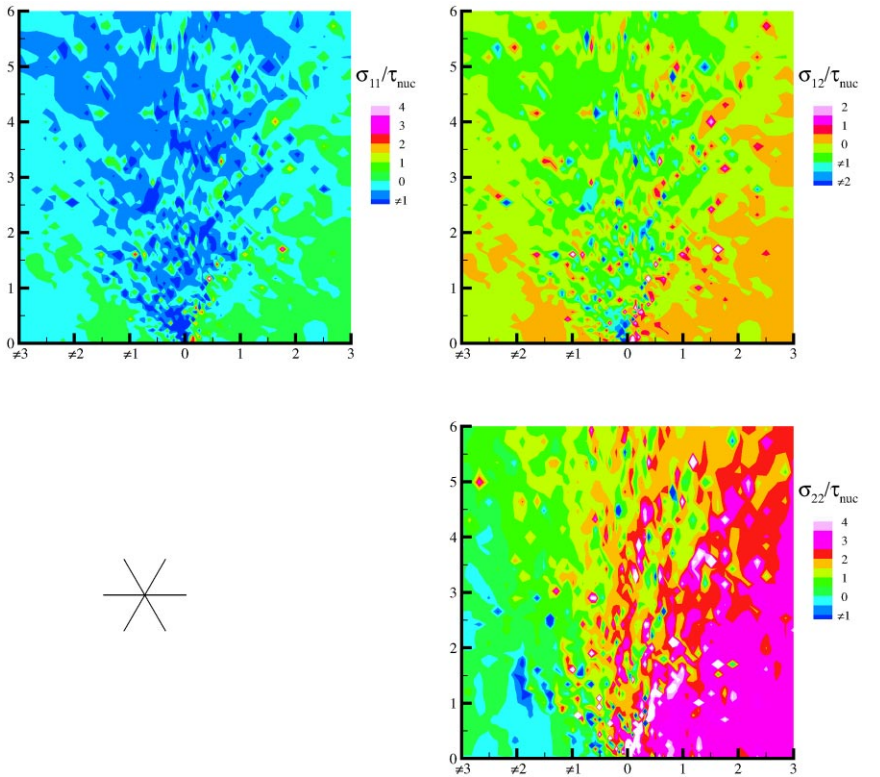

Figure 3 Stress distributions, normalized by the nucleation strength τ_{nuc} in a crystal with three slip systems, as indicated in the inset at $K_I = 0.6$ MPa $\sqrt{m}$. From Van der Giessen et al. (18).

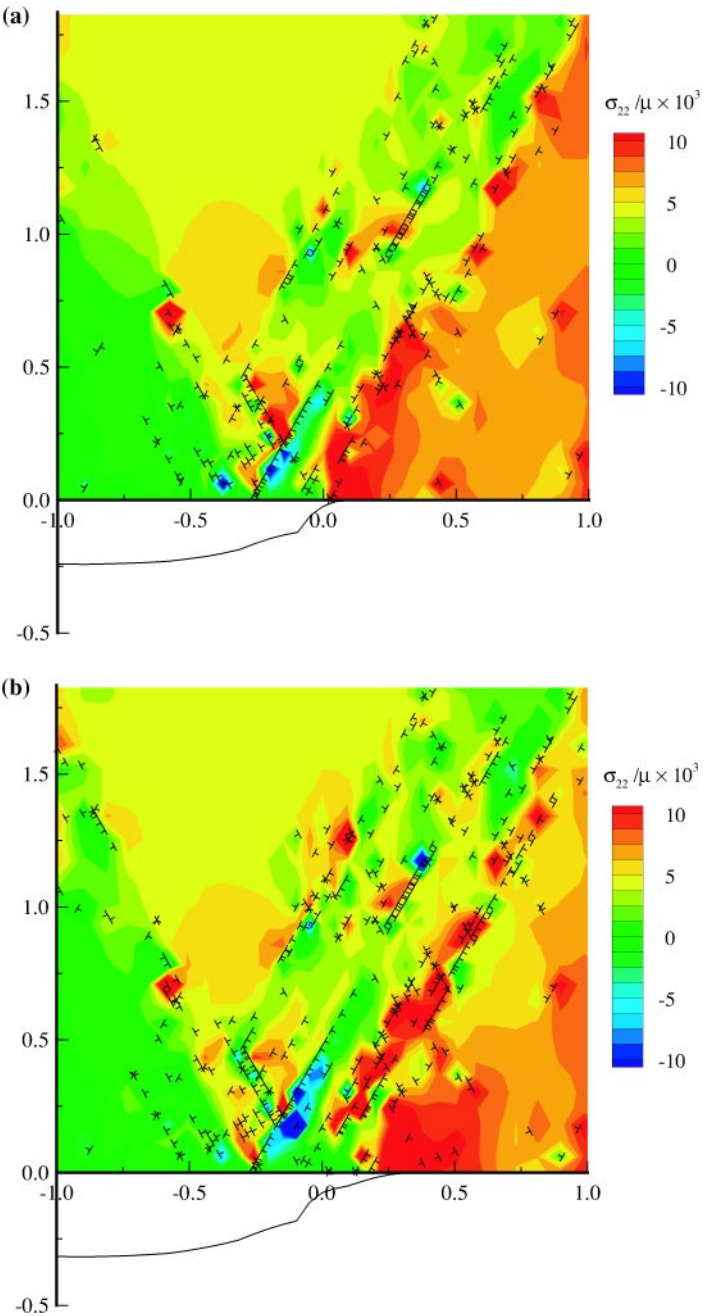

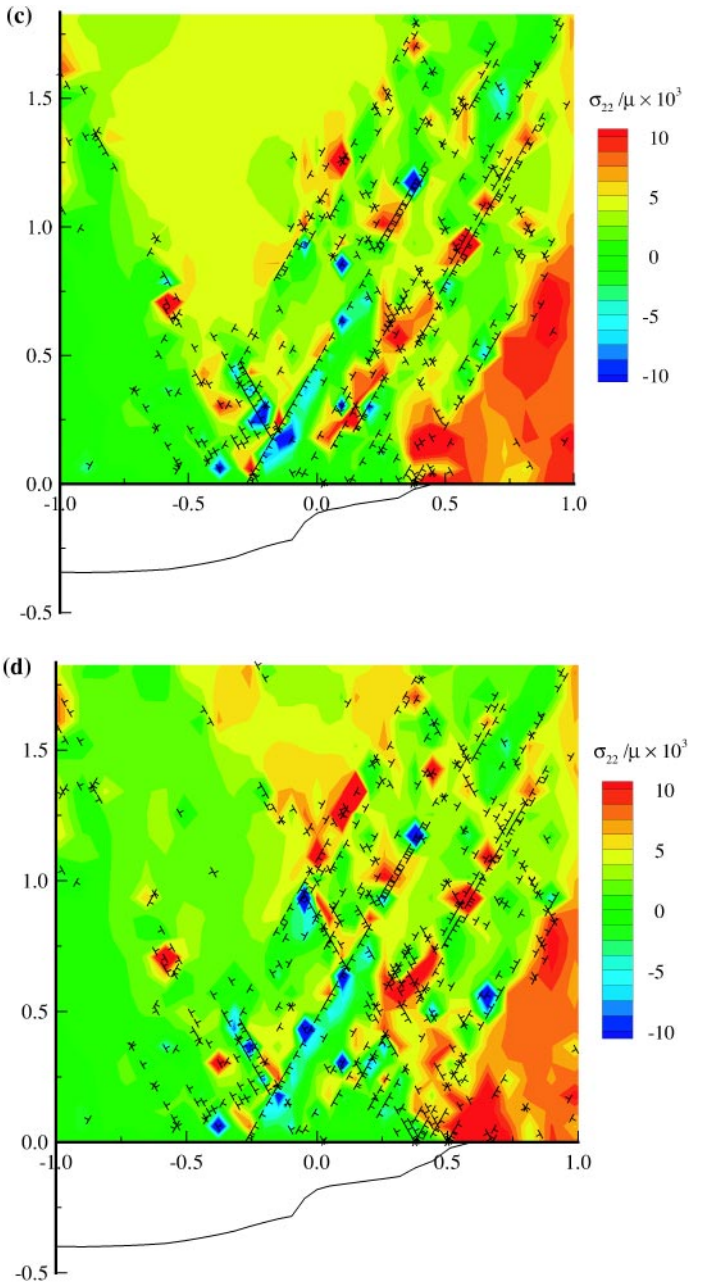

Figure 6 Distribution of dislocations and the opening stress σ_{22} in the immediate neighborhood (2 μm $\times$ 2 μm) of the crack tip for the case with $\rho_{\text{nuc}} = 49/\mu\text{m}^2$ and $\rho_{\text{obs}} = 98/\mu\text{m}^2$ at four different stages of loading. The corresponding crack opening profiles (displacements magnified by a factor of 10) are plotted below the x_1-axis. From Cleveringa et al. (17).